Photoreactivity of $Cr(CO)_4$(2,2′-Bipyridine): Quantum Chemistry and Photodissociation Dynamics

Dominique Guillaumont,[†] Antonin Vlček, Jr.,[‡] and Chantal Daniel*[,†]

Laboratoire de Chimie Quantique, UMR 7551 CNRS/Université Louis Pasteur, 4 Rue Blaise, Pascal F-67 000, France, and Department of Chemistry, Queen Mary and Westfield College (University of London), Mile End Road, London E1 4NS, U.K.

Received: December 20, 1999; In Final Form: June 26, 2000

Metal-to-ligand charge-transfer (MLCT) excited-state dynamics of $Cr(CO)_4$(bpy) (bpy = 2,2′-bipyridine) have been investigated through wave packet propagations on CASSCF/MR-CCI potentials and compared with the results of recent femtosecond time-resolved spectroscopic study. The calculated spectrum is characterized by two peaks, one centered at 21 000 cm^{-1} and assigned to low-lying metal-to-bipyridine charge transfer states, the second one centered at 29 000 cm^{-1} and assigned to a second series of metal-to-bipyridine charge transfer states and to the lowest metal-centered (MC) states. Visible irradiation into the first band brings the molecule in the b^1A_1 MLCT excited state calculated at 21 710 cm^{-1}, with an oscillator strength $f \approx 0.24$ and corresponding to the $3d_{xz} \rightarrow 1\pi^*_{bpy}$ excitation. The evolution of the wave packet along the $Cr-CO_{ax}$ bond elongation shows an ultrafast direct dissociation (in a few hundred femtoseconds) of the axial carbonyl ligand, in agreement with the observed photodissociation dynamics, which points to a carbonyl departure in less than 400 fs. The calculated probability of dissociation of the carbonyl ligand after excitation into the second band is lower than 10% in 1ps.

I. Introduction

Many carbonyl diimine complexes of first-row transition metals have been found to be photoreactive under irradiation into their lowest metal-to-ligand charge-transfer (MLCT) absorption band (metal → α-diimine), the observed primary reaction corresponding to a carbonyl loss.[1−4] The detailed mechanism of CO substitution in this class of molecules sustains a longstanding controversy.[3,5−6] Still, many questions remain unresolved concerning (i) the nature of the reactive excited states (MLCT,MC), (ii) the role of the low-lying triplet excited states, and (iii) the presence and photochemical role of excited states of mixed character either in the Franck−Condon region or along the reaction coordinate.

The $Cr(CO)_4$(bpy) (bpy = 2,2′-bipyridine) complex is a prototype system for the study of carbonyl photodissociation after irradiation into the MLCT band. It has been the subject of a variety of experimental studies in the past decade.[5−10] The UV−visible absorption spectrum of $Cr(CO)_4$(bpy) shows one intense absorption in the visible attributed to a ($3d \rightarrow \pi^*_{bpy}$) MLCT state[1b,1c,8,11,12] and another one in the UV region originating in strongly overlapping absorption bands due to closely spaced transitions into MLCT and MC states.[11] A weak shoulder at about 400 nm appears between these strong groups of bands. Traditionally, it was attributed to a MC transition (note that a LF (ligand field) notation is often used in the literature for states denoted therein as MC, metal-centered). The energy of the visible band is solvent dependent and is attributed to MLCT transitions. In solution, photosubstitution of the axial CO ligand has been observed

$$Cr(CO)_4(bpy) \xrightarrow[L]{h\nu} fac\text{-}Cr(CO)_3(L)(bpy) + CO \qquad (1)$$

The quantum yield ϕ_{sub} of the photosubstitution (eq 1) has been measured as a function of the irradiation wavelength varied within the range of the MLCT absorption.[6] After irradiation into the high-energy domain (21 000 $cm^{-1} < E_{ex} < 28\,000$ cm^{-1}), ϕ_{sub} increases significantly with the excitation energy ($\phi_{sub} = 0.06$ at 21 800 cm^{-1}, $\phi_{sub} = 0.2$ at 27 600 cm^{-1}). Visible irradiation (16 100 $cm^{-1} < E_{ex} < 21\,000$ cm^{-1}) is characterized by a slow, nearly linear increase of the quantum yield with the excitation energy ($\phi_{sub} = 0.02$ at 16 300 cm^{-1}, $\phi_{sub} = 0.06$ at 20 120 cm^{-1} in C_6H_6). Moreover, the quantum yield measured using visible excitation is temperature-dependent with apparent activation energies of 1350 and 1430 cm^{-1} at $E_{ex} = 20\,210$ and 17 950 cm^{-1}, respectively.[6]

The excited-states dynamics of $Cr(CO)_4$(bpy) have been investigated using pump−probe time-resolved absorption spectroscopy in solutions (S = pyridine, CH_2Cl_2).[13] Excitation by tunable laser pulses (with a width of ca. 250 fs) into the strong MLCT ($3d_{Cr} \rightarrow \pi^*_{bpy}$) band (560−720 nm) has shown the following features:

(i) formation of the $Cr(S)(CO)_3$(bpy) photoproduct within 600 fs, that is, with a time constant less than 400 fs;

(ii) population of two trapping excited states parallel to CO dissociation;

(iii) decay of these two unreactive states in pyridine in 8 and 87 ps.

The branching ratio between the reactive (CO loss) and unreactive channels (relaxation to the unreactive states) decreases with decreasing excitation energy in the range of MLCT absorption.

The goal of the present study is to propose a photodissociation mechanism for the CO departure from MLCT excited $Cr(CO)_4$-

* Corresponding author.
[†] Université Louis Pasteur.
[‡] Queen Mary and Westfield College.

10.1021/jp994435o CCC: $20.00
Published on Web 01/27/2001

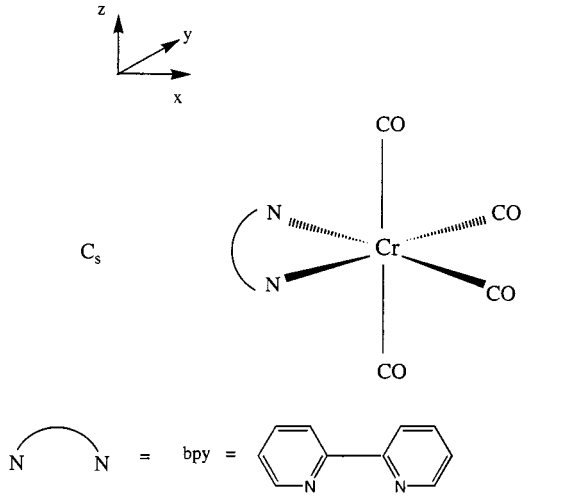

Figure 1. Idealized structure of $Cr(CO)_4(bpy)$.

SCHEME 1

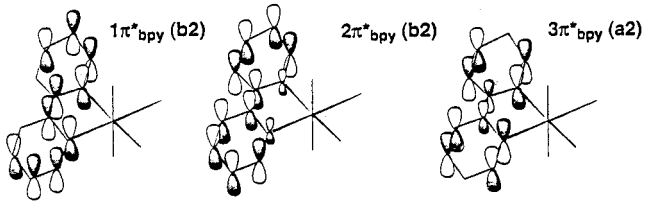

(bpy) on the basis of wave packet propagations on ab initio electronic ground and excited-state potentials calculated as a function of the reaction coordinate corresponding to the axial CO ligand loss. Investigation of fast elementary processes participating in the photodissociation of a number of organometallics using a time-dependent approach and based on ab initio potential energy surfaces has been the subject of recent studies.[14−16] The theoretical study described below aims at investigating the elementary processes occurring between the initial excitation and the formation of the $Cr(CO)_3(bpy)$ primary products determined experimentally. The ultimate goal is to build a link between experiments and simulations in order to unravel the nature of processes occurring between 0 and 1 ps. The simulations reported in the present work are essentially Franck−Condon simulations corresponding to the overall absorption spectrum and are not directly comparable to the pump/probe experiments performed in condensed phase. Moreover, solvent effects not taken into account here could lead to inhomogeneous broadening.

II. Computational Details

Quantum Chemical Calculations. The C_{2v} geometry of $Cr(CO)_4(bpy)$ has been idealized from the experimental structures of $[Ru(bpy)_3]^{2+}$ [17] and $Cr(CO)_6$[18] (Figure 1), the bond distances and angles being those used in the previous DV-Xα [19] and CASPT2 studies.[11]

The electronic configuration of the molecule in its $^1A_1$ electronic ground state is given by

$$(3d_{x^2-y^2})^2(3d_{yz})^2(3d_{xz})^2$$

The $3d_{x^2-y^2}$, $3d_{xz}$, and $3d_{yz}$ molecular orbitals are mainly localized on the metal center. The lowest unoccupied orbitals are three π^*_{bpy} orbitals localized on the bpy ligand (denoted $1\pi^*_{bpy}$, $2\pi^*_{bpy}$, and $3\pi^*_{bpy}$) (Scheme 1), the π^*_{CO} orbitals are localized on the carbonyl ligands, and the $3d_{xy}$ and $3d_z^2$ orbitals are localized on the metal center. Three types of low-energy electronic excited states can be distinguished: (i) chromium to bipyridine MLCT states corresponding to the $3d \rightarrow \pi^*_{bpy}$ excitations; (ii) chromium to carbonyl MLCT states corresponding to the $3d \rightarrow \pi^*_{CO}$ excitations; and (iii) MC corresponding to $3d \rightarrow 3d$ excitations. Consequently, the electronic spectrum of $Cr(CO)_4(bpy)$ is characterized by a high density of various electronic states. The first step of the theoretical study is to select states which are accessible directly through vertical excitation (either visible or near-UV) of high oscillator strengths from the $^1A_1$ electronic ground state. On the basis of the calculated excitations energies and oscillator strengths, only a few singlet states are selected for the calculation of the potential energy curves along the Cr−CO axial bond elongation. Since the present work deals with ultrafast processes (subpicosecond), the role of the triplet states will be the object of another study. Indeed, it has been shown recently that the time scale of dissociation via singlet to triplet intersystem crossing processes is not competitive with the direct fast dissociation from the singlet in a number of organometallics (a few tens of picoseconds in the former case versus a few hundreds of femtoseconds in the latter one).[16,20]

The basis sets, which are of generally contracted atomic natural orbital (ANO) type, are the following:[21] for the chromium atom, a (17s12p9d) set contracted to [6s4p3d]; for the first-row atoms, a (10s6p) set contracted to [3s2p]; and for the hydrogen atoms, a (7s) set contracted to [2s].

The ab initio calculations have been performed at the correlated level. Complete active space SCF (CASSCF) calculations were carried out to obtain wave functions, which are used as references in the multireference contracted configuration interaction (CCI). In a previous study,[11] we have calculated vertical excitation energies at the CASSCF/CASPT2 level. Because of the size of the molecule and of the presence of several interacting states along the reaction coordinate, the CASSCF/MR-CCI method turned out to be more appropriate for the calculation of the potential energy curves.

CASSCF wave functions were optimized for a high-spin state ($S = 4$). Two types of CASSCF wave functions have been used on the basis of different active spaces. The first one, the so-called 6e17a, in which 6 electrons are correlated in 17 active orbitals, includes the 3d orbitals occupied in the electronic ground state ($3d_{x^2-y^2}$ (b_1), $3d_{yz}$ (a_2), $3d_{xz}$ (a_1)) and the 3d orbitals which correlate them, the three low-lying π^*_{bpy} ($1\pi^*_{bpy}$ (b_2), $2\pi^*_{bpy}$ (b_2), $3\pi^*_{bpy}$ (a_2)) (see Scheme 1) and the low-lying π^*_{CO} vacant orbitals. The second wave function has been obtained through the so-called 10e12a CASSCF calculation (10 electrons correlated in 12 active orbitals), which includes all the 3d orbitals (occupied or vacant in the electronic ground state), the 3d of correlation, the two low-lying π^*_{bpy} orbitals, and two occupied orbitals with a significant contribution on the metal center. This second calculation has been used only for the calculation of the MC states corresponding to 3d excitations.

For each electronic state corresponding to $3d \rightarrow \pi^*_{bpy}$ excitations, a monoreference CI calculation is performed followed by a MR- CCI calculation, including references appearing with a coefficient >0.08 in the MR-CCI. Single and double excitations to all virtual orbitals, except the counterparts of the carbonyls and diimine 1s and of the metal 1s, 2s, and 2p orbitals, are included. The transition dipole moments have been evaluated at the CASSCF, the calculations being performed with the MOLCAS-3 quantum chemistry software.[22]

The potential energy curves as a function of the $Cr-CO_{ax}$ bond elongation have been calculated under the C_s symmetry

SCHEME 2

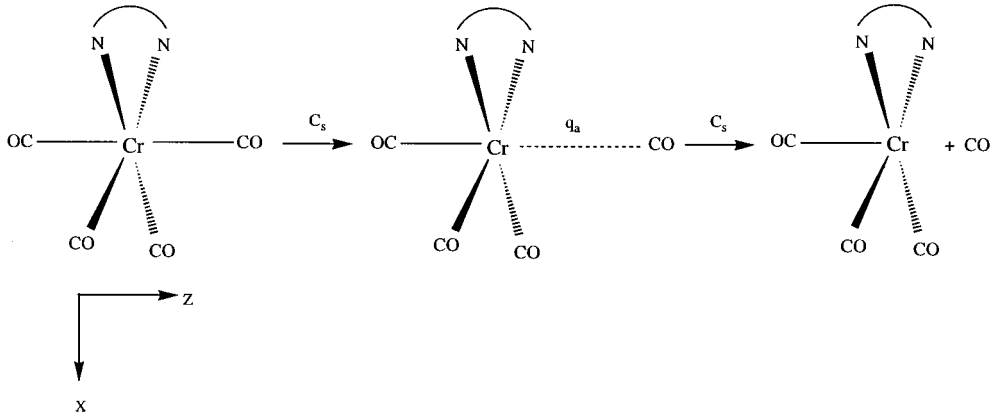

constraint. Owing their complexity and their, cost these calculations have been restricted to the a^1A_1 electronic ground state and to the six low-lying excited states corresponding to the $a^1A_1 \rightarrow {}^1A_1$, $a^1A_1 \rightarrow {}^1B_1$, and $a^1A_1 \rightarrow {}^1B_2$ allowed transitions assigned to $3d_{Cr} \rightarrow \pi^*_{bpy}$ excitations.

Photodissociation Dynamics. For the sake of simplicity, the molecule is modeled as pseudodiatomic with one dissociative bond $q_a = [Cr-CO_{ax}]$ (Scheme 2). All other spectator modes are decoupled in this zero-order approximation. This decoupling mode should be reasonable, at least for ultrafast time scales (less than 1 ps) when energy remains in the dissociative bond. Moreover, expriments indicate that the primary products of reaction 1 have the solvent molecule in axial position.

The simulation of the photodissociation dynamics is based on the resolution of the time-dependent Schrödinger equation. Selected nuclear wave packets $\chi(q_a,t)$ are propagated in time on the excited-state potentials

$$i\hbar\frac{\partial}{\partial t}\chi_e(q_a,t) = \hat{H}\chi_e(q_a,t) \tag{1}$$

with the following initial conditions:

$$\chi_e(q_a,t=0) = \mu_e\Psi_{gs}(q_a) \tag{2}$$

where μ_e is the electronic transition dipole moment between the ground state (gs) and the excited-state e. Ψ_{gs} represents the vibrational wave function of the electronic ground state corresponding to the $Cr-CO_{axial}$ stretching normal mode. It is evaluated through the Fourier Grid Hamiltonian method.[23]

$\hat{H}$ is the Hamiltomian of the system

$$\hat{H} = \hat{T}_{nu} + V_e \tag{3}$$

where V_e is the potential of the excited state which has been calculated by ab initio calculations and $\hat{T}_{nu}$ is the kinetic operator

$$\hat{T}_{nu} = \frac{-\hbar^2}{2\mu_a}\frac{\partial^2}{\partial q_a} \tag{4}$$

$\mu_a = (m_{Cr}m_{CO})/(m_{Cr} + m_{CO})$ is the reduced mass corresponding to the bond $q_a = [Cr-CO_{ax}]$.

According to the time-dependent formalism,[24] the absorption spectrum $\sigma(\omega)$ is given by the Fourier transform of the autocorrelation function $S(t)$

$$\sigma(\omega) \propto \omega\int_{-\infty}^{+\infty} dt\, e^{i(E_i+\hbar\omega)t/\hbar}S(t) \tag{5}$$

where

$$S(t) = \langle\chi_e(0)|\chi_e(t)\rangle \tag{6}$$

and E_i represents the energy of the initial wave packet.

The dissociation probability corresponding to the fraction of the wave packet that has passed the dissociation limit (defined by the internuclear distance q_{diss}) at time t is determined by

$$P_{diss}(t) = 1 - \int_{q_0}^{q_{diss}} |\chi_e(q_a,t)|^2\, dq_a \tag{7}$$

The solution of the time-dependent Schrödinger equation (eq 1) is obtained by the fourth-order differencing (FOD) scheme,[25] with $\Delta t = 0.007\,26$ fs.

Potentials and wave packets are represented on a one-dimensional grid corresponding to the reaction coordinate with the following parameters: $q_{a_i} = q_{a_0} + (i-1)\Delta q_a$, $q_{a_0} = 1.6$ Å, and $\Delta q_a = 0.025$ Å, with $1 \le i \le 512$.

III. Results

Excited States. Qualitative CASSCF excitation energies calculated for the low-lying singlet MLCT ($3d_{Cr} \rightarrow \pi^*_{bpy}$), MLCT ($3d_{Cr} \rightarrow \pi^*_{CO}$), and MC ($3d_{Cr} \rightarrow 3d_{Cr}$) excited states of $Cr(CO)_4$(bpy), and the associated dipole transition moments are reported in Table 1. The purpose of these preliminary CASSCF calculations in which important dynamical correlation effects (which may account for a lowering of the excitation energies by a few thousands of wavenumbers) are not included is to determine the main contributions to the visible and near-UV absorption spectra and to investigate the relative position of the different types of excited states.

According to these results, the lowest part of the spectrum consists of three MLCT transitions, $^1A_1 \rightarrow {}^1B_2$, $^1A_1 \rightarrow {}^1B_1$, and $^1A_1 \rightarrow {}^1A_1$, atttributed to $3d_{Cr} \rightarrow 1\pi^*_{bpy}$ excitations. The $^1B_2$ state has a very small dipole transition moment, while the $^1B_1$ and $^1A_1$ states should contribute significantly to the first intense band regarding their relatively high transition dipole moments of 0.59 and 1.65 au, respectively. The next four transitions correspond to 3dCr $\rightarrow \pi^*_{CO}$ excitations; two of them are symmetry-forbidden ($^1A_2$), and the two others ($^1A_1 \rightarrow {}^1B_1$ and $^1A_1 \rightarrow {}^1B_2$) have smaller dipole transition moments. The middle part of the spectrum is composed essentially of four closely spaced states assigned to $3d_{x^2-y^2} \rightarrow 2\pi^*_{bpy}$, $3d_{x^2-y^2} \rightarrow 3\pi^*_{bpy}$, and $3d_{Cr} \rightarrow \pi^*_{Co}$ excitations with rather modest dipole transition moments. The second intense band band observed experimentally in the UV should correspond to the superposition of four

TABLE 1: CASSCF Excitation Energies (in cm^{-1}) to the Low-Lying MLCT States ($3d_{Cr} \rightarrow \pi^*_{bpy}$ and $3d_{Cr} \rightarrow \pi^*_{CO}$) and MC States ($3d_{Cr} \rightarrow 3d_{Cr}$) of $Cr(CO)_4$(bpy) and Associated Dipole Transition Moments (in au)

	one-electron excitation in the principal configuration	CASSCF **6e17a**[a] CASSCF**10e12**[b]	μ
$^1B_2$	$3d_{x^2-y^2} \rightarrow 1\pi^*_{bpy}$	19770	0.02
$^1B_1$	$3d_{yz} \rightarrow 1\pi^*_{bpy}$	22150	0.59
$^1A_1$	$3d_{xz} \rightarrow 1\pi^*_{bpy}$	24310	1.65
$^1A_2$	$3d_{yz} \rightarrow \pi^*_{CO}$	25900	0.00
$^1A_2$	$3d_{xz} \rightarrow \pi^*_{CO}$	26720	0.00
$^1B_1$	$3d_{x^2-y^2} \rightarrow \pi^*_{CO}$	27600	0.28
$^1B_2$	$3d_{yz} \rightarrow \pi^*_{CO}$	27940	0.27
$^1B_2$	$3d_{x^2-y^2} \rightarrow 2\pi^*_{bpy}$	30083	0.00
$^1A_1$	$3d_{x^2-y^2} \rightarrow \pi^*_{CO}$	31000	0.00
$^1A_2$	$3d_{x^2-y^2} \rightarrow 3\pi^*_{bpy}$	31800	0.00
$^1B_1$	$3d_{yz} \rightarrow 2\pi^*_{bpy}$	31870	0.48
$^1A_1$	$3d_{yz} \rightarrow 3\pi^*_{bpy}$	33110	0.85
$^1A_1$	$3d_{xz} \rightarrow 2\pi^*_{bpy}$	33600	0.88
$^1B_2$	$3d_{x^2-y^2} \rightarrow \pi^*_{CO}$	33950	0.01
$^1B_1$	$3d_{x^2-y^2} \rightarrow 3d_{xy}$	34190	0.80
$^1B_1$	$3d_{xz} \rightarrow 3\pi^*_{bpy}$	34957	1.35
$^1A_1$	$3d_{x^2-y^2} \rightarrow \pi^*_{CO}$	38000	0.38
$^1B_2$	$3d_{yz} \rightarrow 3d_{xy}$	38540	0.52
$^1A_1$	$3d_{yz} \rightarrow \pi^*_{CO}$	39660	0.30
$^1A_1$	$3d_{x^2-y^2} \rightarrow 3d_{z^2}$	42830	0.28
$^1B_2$	$3d_{xz} \rightarrow 3d_{z^2}$	42930	0.07

[a] CASSCF performed for the MLCT states. [b] CASSCF performed for the MC states.

MLCT transitions, corresponding to $3d_{Cr} \rightarrow 2\pi^*_{bpy}$ and $3d_{Cr} \rightarrow 3\pi^*_{bpy}$ excitations, and of the MC state $3d_{x^2-y^2} \rightarrow 3d_{xy}$, which possess dipole transition moments between 0.48 and 1.35 au. The upper part of the absorption spectrum is made up of a series of MC and a few MLCT ($3d_{Cr} \rightarrow \pi^*_{CO}$) states, which should not participate to the visible or near-UV photochemistry investigated here.

According to the results of the preliminary CASSCF calculations reported in Table 1, relatively low transition dipole moments are associated to the MLCT ($3d_{Cr} \rightarrow \pi^*_{CO}$) states in $Cr(CO)_4$(bpy). Consequently, these states should not contribute significantly to the absorption and to the ultrafast dynamical events occurring after vertical transition in the Franck−Condon region. For this reason, their investigation will not be carried out further. However, the MLCT ($3dCr \rightarrow \pi^*_{CO}$) transitions could contribute to the weak shoulder observed in the spectra at about 400 nm (21 000−27 000 cm^{-1}). The MR-CCI calculated vertical excitation energies to the lowest singlet states corresponding to the MLCT ($3d_{Cr} \rightarrow 1\pi^*_{bpy}$, $3d_{Cr} \rightarrow 2\pi^*_{bpy}$, $3d_{Cr} \rightarrow 3\pi^*_{bpy}$) transitions are reported in Table 2, together with the oscillator strengths.

Despite the high density of states which characterizes the lowest part of the theoretical spectrum of this molecule, only two states have large oscillator strengths (>0.10): the b^1A_1 state, corresponding to the $3d_{xz} \rightarrow 1\pi^*_{bpy}$ calculated at 21 710 cm^{-1} with an oscillator strength of 0.17, and the b^1B_1 state, corresponding to the $3d_{xz} \rightarrow 3\pi^*_{bpy}$ calculated at 29 570 cm^{-1} with and oscillator strength of 0.16. The other allowed transitions with nonzero oscillator strengths are calculated at 18 280 cm^{-1}, 28 550 cm^{-1}, and 30 720 cm^{-1} and correspond to the a^1B_1 ($3d_{yz} \rightarrow 1\pi^*_{bpy}$), c^1A_1 ($3d_{yz} \rightarrow 3\pi^*_{bpy}$), and d^1A_1 ($3d_{xz} \rightarrow 2\pi^*_{bpy}$) states, respectively. The two low-lying states range into the visible energy domain, while the others are situated in the near UV region and separated from the previous ones by nearly 1 eV.

TABLE 2: CASPT2 and MR-CCI Excitation Energies (in cm^{-1}) to the Low-Lying MLCT ($3d_{Cr} \rightarrow \pi^*_{bpy}$) and MC ($3d_{Cr} \rightarrow 3d_{Cr}$) Excited States of $Cr(CO)_4$(bpy) and Associated Oscillator Strengths

transitions	one-electron excitation in the principal configuration	CASPT2[c]	MRCI	f
$a^1A_1 \rightarrow a^1B_2$	$3d_{x^2-y^2} \rightarrow 1\pi^*_{bpy}$	12630	17300	0.00[a]−0.00[b]
$a^1A_1 \rightarrow a^1B_1$	$3d_{yz} \rightarrow 1\pi^*_{bpy}$	14450	18280	0.02[a]−0.02[b]
$a^1A_1 \rightarrow b^1A_1$	$3d_{xz} \rightarrow 1\pi^*_{bpy}$	17580	21710	0.17[a]−0.24[b]
$a^1A_1 \rightarrow a^1A_2$	$3d_{x^2-y^2} \rightarrow 3\pi^*_{bpy}$		26930	0.00[a]
$a^1A_1 \rightarrow c^1A_1$	$3d_{yz} \rightarrow 3\pi^*_{bpy}$	25370	28550	0.06[a]−0.12[b]
$a^1A_1 \rightarrow b^1B_1$	$3d_{xz} \rightarrow 3\pi^*_{bpy}$	26200	29570	0.16[a]−0.13[b]
$a^1A_1 \rightarrow b^1B_2$	$3d_{x^2-y^2} \rightarrow 2\pi^*_{bpy}$		29700	0.00[a]
$a^1A_1 \rightarrow d^1A_1$	$3d_{xz} \rightarrow 2\pi^*_{bpy}$		30720	0.07[a]
$a^1A_1 \rightarrow c^1B_1$	$3d_{yz} \rightarrow 2\pi^*_{bpy}$		31000	0.02[a]
$a^1A_1 \rightarrow d^1B_1$	$3d_{x^2-y^2} \rightarrow 3d_{xy}$	29650		
$a^1A_1 \rightarrow c^1B_2$	$3d_{yz} \rightarrow 3d_{xy}$	32230		
$a^1A_1 \rightarrow d^1B_2$	$3d_{xz} \rightarrow 3d_{z^2}$	36320		
$a^1A_1 \rightarrow e^1A_1$	$3d_{x^2-y^2} \rightarrow 3d_{z^2}$	37360		

[a] Values obtained on the basis of the 6e17a CASSCF wave function ($S = 4$). [b] Values obtained on the basis of the 10e12a CASSCF wave function ($S = 4$). [c] From ref 11.

The CASPT2 excitation energies[11] to the MC states corresponding to the $3d_{Cr}$ to $3d_{Cr}$ excitations are also reported in Table 2. These states have very low oscillator strengths, range in the UV energy domain, and should not contribute significantly to the absorption spectrum. Since we are mostly interested by the MLCT reactivity, these states are excluded from the simulation of the dynamics. However, one has to point to the near-degeneracy of the d^1B_1 MC state with the d^1A_1 MLCT state, which could affect the UV photoreactivity of the complex and which will be investigated more in detail in another study.

Potential Energy Curves for the Axial CO Loss. Potential energy curves along the $Cr-CO_{axial}$ bond elongation were determined at the CASSCF/MR-CCI level for the ground state, the three lowest excited states, and the states with a high value of transition dipole moment, namely, the a^1B_1, a^1B_2, and b^1A_1 MLCT states belonging to the visible region and the c^{1}A1, b^{1}B1, and d^{1}A1 MLCT states situated in the near-UV region. The a^1A_2, b^1B_2 and c^1B_1 states have been excluded from the present simulation. This reaction pathway has been studied under C_s symmetry constraint (Scheme 1).

The calculated CASSCF/MR-CCI values are reported in Table 3, and the corresponding potential energy curves are displayed in Figure 2. The d^1A_1 state represented in dot line have been obtained with a poor accuracy due to convergence problems in the CI calculations for the highest solutions.

The three lowest MLCT states, a^1B_2, a^1B_1, and b^1A_1, corresponding to the $3d \rightarrow 1\pi^*_{bpy}$ excitations, were calculated to be very weakly bound. The MLCT character of these states decreases with the $Cr-CO_{axial}$ bond elongation. The $3d_{z^2}$ orbital is stabilized and interacts with the $1\pi^*_{bpy}$ orbital to form $1\pi^*_{bpy} + 3d_{z^2}$ and $1\pi^*_{bpy} - 3d_{z^2}$ mixed orbitals. In term of electronic states, an avoided crossing appears between the MLCT ($3d \rightarrow 1\pi^*_{bpy}$) and the MC ($3d \rightarrow 3d_{z^2}$) states. At dissociation, the electronic character of the lowest excited states is a mixing MLCT/MC with more MLCT character, and MC/MLCT states are pushed up to higher energies. This situation of avoided crossings between MLCT and MC states along a metal−CO bond has also been shown through DFT calculations for the $Mn(Cl)(CO)_3$(H-DAB) complex.[26]

The nearly dissociative character of the low-lying MLCT states associated with a weakening of the metal−carbonyl bond

TABLE 3: CASSCF/MR-CCI Energies (in au with respect to −1986) of the Singlet Excited States Contributing Significantly to the Absorption Spectrum of $Cr(CO)_4$(bpy) as a Function of the $Cr-CO_{ax}$ Bond Elongation

$Cr-CO_{ax}$ (Å)	a^1A_1	a^1B_2	a^1B_1	b^1A_1	c^1A_1	b^1B_1	d^1A_1
1.6	0.12379	0.04404	0.02241	0.01616	0.98472	0.98591	0.9700
1.92	0.20782	0.12900	0.12449	0.10888	0.07771	0.07307	0.06785
2.2	0.20405	0.14101	0.13976	0.12303	0.09039	0.08658	
2.5	0.19525	0.14000	0.14102	0.12437	0.08916	0.09131	0.0840
3.5	0.17916	0.13756	0.13880	0.12358	0.08001	0.08334	0.077
50.0	0.17044	0.12998	0.13397	0.11972	0.07270	0.075	

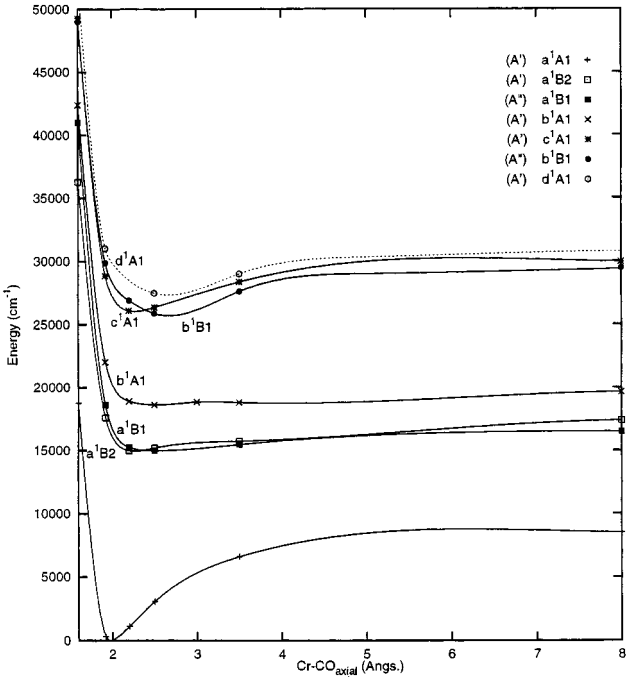

Figure 2. CASSCF/MR-CCI potential energy curves as a function of the $Cr-CO_{ax}$ bond elongation in $Cr(CO)_4$(bpy) calculated under C_s symmetry constraint.

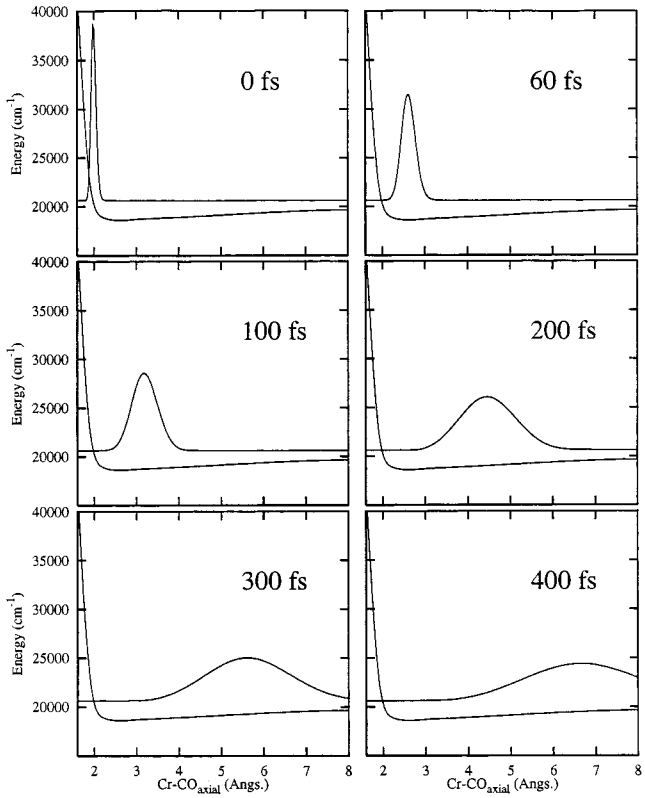

Figure 3. Time-evolution of the $\chi_{b^1A_1}(q_a,t)$ wave packet (dashed line) on the potential $V_{b^1A_1}(q_a)$ (continuous line), where $q_a = [Cr - CO_{ax}]$.

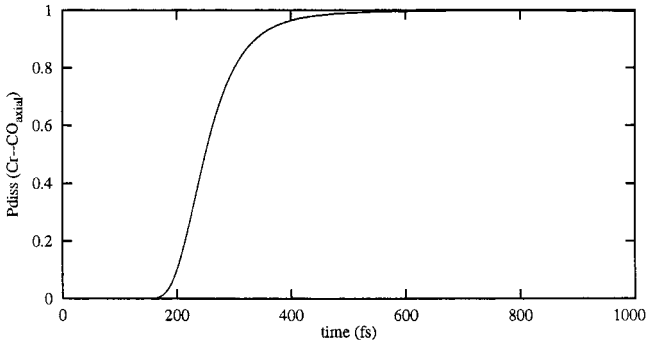

Figure 4. Probability of dissociation of the axial CO in $Cr(CO)_4$(bpy) as a function of time after population of the b^1A_1 MLCT excited state by irradiation into the visible.

was already shown for $M(R)(CO)_3$(H-DAB)[15,16] complexes. In the manganese complex $Mn(H)(CO)_3$(H-DAB), this feature has been explained by the decrease of the $d\pi-p\pi$ back-donation between the metal and the axial carbonyl ligand when going from the electronic ground state to the MLCT states in first-row transition-metal complexes.[16] In contrast to the low-lying MLCT states absorbing in the visible energy domain, the upper MLCT states c^1A_1, b^1B_1, and d^1A_1 belonging to the near-UV region are nearly quasibound and should not be very reactive.

Photodissociation Dynamics. The excited-state dynamics are simulated according to three schemes: (i) after excitation to the singlet states in the visible region of the spectrum, which corresponds to MLCT absorption; (ii) after the excitation to the singlet excited states belonging to the near-UV region; (iii) after the initial excitation to all singlet states in order to simulate the absorption spectrum.

Visible Irradiation. The wave packet is propagated on the b^1A_1 MLCT state calculated at 21 710 cm^{-1} with a high transition dipole moment (>1.6 au) with the following initial conditions:

At time $t = 0$, the wave packet is the vibrational ground state of the electronic ground state

$$\chi_{b^1A_1}(q_a,t=0) = \Psi_{a^1A_{1,0}}(q_a)$$

The evolution of the wave packet on the b^1A_1 potential as function of time is represented by snapshots of the densities $|\chi_{b^1A_1}(q_a,t)|^2$ in Figure 3. The initial excitation transfers the wave packet on the repulsive part of the MLCT potential. The wave packet dissociates entirely in the direction of the carbonyl loss. In less than 500 fs, all the amplitude of the wave packet has gone through the dissociation limit, indicating a fast and complete reaction.

The carbonyl loss probability as a function of time is displayed in Figure 4.

UV Irradiation. The c^1A_1 and b^1B_1 states calculated between 28 5500 and 29 570 cm^{-1} are the best candidates for UV

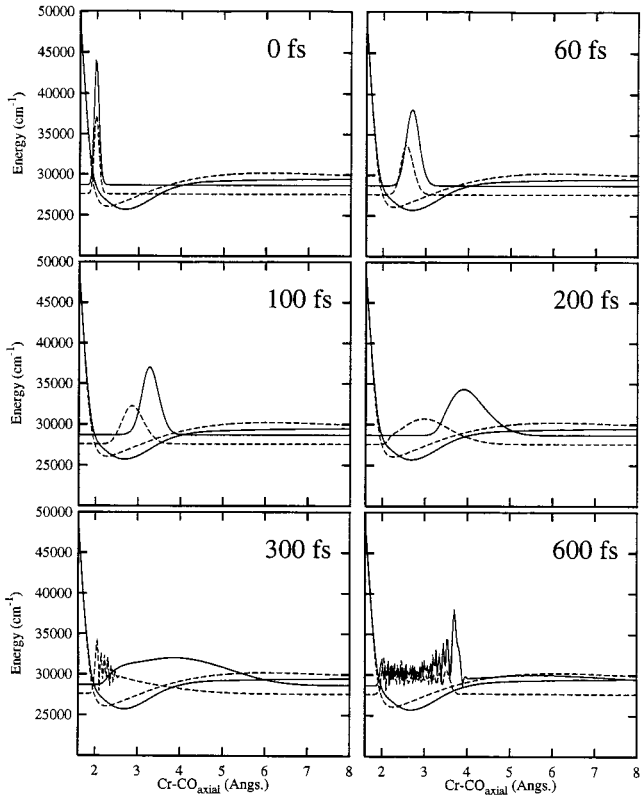

Figure 5. Time evolution of the $\chi_{c^1A_1}(q_a,t)$ (dashed line) and $\chi_{b^1B_1}(q_a,t)$ (continuous line) wave packets on the potentials $V_{c^1A_1}(q_a)$ (dashed line) and $V_{b^1B_1}(q_a)$ (continuous line), where $q_a = [Cr-CO_{ax}]$.

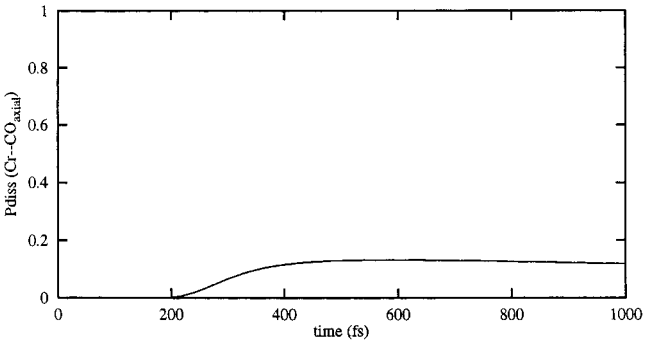

Figure 6. Probability of dissociation of the axial CO in $Cr(CO)_4(bpy)$ as a function of time after population of the c^1A_1 and b^1B_1 MLCT excited states by irradiation into the near-UV region.

irradiation. The d^1A_1 state is excluded from the simulation due to inaccuracy in the calculation of the associated potential.

At the initial time, the vibrational state of the electronic ground state is transferred to the two MLCT states

$$\mu_{a^1A_1 \rightarrow c^1A_1} = 0.85$$

$$\mu_{a^1A_1 \rightarrow c^1B_1} = 1.35$$

$$\chi_{c^1A_1}(q_a, t=0) = 0.85\Psi_{a^1A_{1,0}}(q_a)$$

$$\chi_{b^1B_1}(q_a, t=0) = 1.35\Psi_{a^1A_{1,0}}(q_a)$$

The time evolution of the initial wave packet on the corresponding potentials is represented by the snapshots in Figure 5.

The major part of the wave packet gets trapped into the potential wells of the two MLCT states in the Franck−Condon region. Ten percent of the wave packet dissociates in less than 500 fs from the b^1B_1 state. The carbonyl dissociation probability is given in Figure 6.

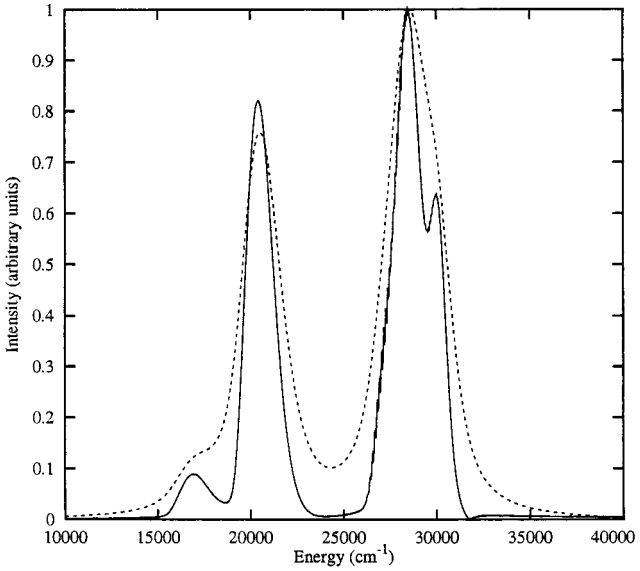

Figure 7. Theoretical absorption spectrum of $Cr(CO)_4(bpy)$ obtained by the Fourier Transform of the original autocorrelation function multiplied by an exponential factor $\exp(-\Gamma t)$, with $\Gamma = 0.02$ (continuous line) and $\Gamma = 0.13$ (dashed line).

Absorption Spectrum. The absorption spectrum is simulated by propagations of the selected initial wave packet on the six potentials represented in Figure 2 and corresponding to the six low-lying MLCT ($d \rightarrow \pi^*_{bpy}$) excited states of $Cr(CO)_4(bpy)$. To reproduce correctly the intensity of absorption bands, we take into account the potential of the d^1A_1 state, even if it is not accurate. If the shape of the potential may influence strongly the dissociation probability, its effect is presumed to be less important on the simulation of an absorption band.

At the initial time, the vibrational state of the electronic ground state is simultaneously transferred to the singlet excited states, after multiplication by transition moment values.

The autocorrelation function is multiplied by an exponential function $\exp(-\Gamma t)$, where Γ is a phenomenological lifetime.

The simulated spectrum represented in Figure 7 shows two intense absorption bands centered at 20 500 and 28 500 cm^{-1}. The position of these bands is approximately 1000 cm^{-1} lower than vertical MR-CCI excitation energies reported in Table 2. This is due to the repulsive shape of the potentials in the Franck−Condon region.

The UV−visible absorption spectrum of $Cr(CO)_4(bpy)$ exhibits an intense absorption band in the visible region (500 nm or 20 000 cm^{-1}) and an even stronger absorption band in the UV region (330 nm or 30 300 cm^{-1}). The position of the visible absorption band is strongly solvent-dependent. For instance, this band attributed to MLCT transitions has been measured at 17 700 cm^{-1} in C_2Cl_4/C_6H_6 6/1 (v/v). Near-UV absorption is poorly resolved but in C_2Cl_4/C_6H_6, an absorption band appears at 25 800 cm^{-1}, and a shoulder is observed around 400 nm (25 000 cm^{-1}), whatever the solvent is.

The first absorption band, measured at 17 700 cm^{-1} in C_2Cl_4/C_6H_6, can be mainly assigned to $3d_{xz} \rightarrow 1\pi^*_{bpy}$ transition simulated at 20 500 cm^{-1}.

The second absorption band, measured at 25 800 cm^{-1} in C_2Cl_4/C_6H_6, cannot be assigned easily on the basis of the present simulation, which excludes the MLCT transitions corresponding to $3d_{Cr} \rightarrow \pi^*_{CO}$ excitations. The strong absorption centered 28 500 cm^{-1} is assigned to MLCT transitions corresponding to

the $3d_{yz} \rightarrow 3\pi^*_{bpy}$, $3d_{xz} \rightarrow 3\pi^*_{bpy}$, and $3d_{xz} \rightarrow 2\pi^*_{bpy}$ excitations. It is worth noting that a number of states belong to the visible near-UV region with non-negligible oscillator strengths (Table 2), each state bringing a small contribution to the spectrum which is not included in the present simulation. Inaccuracy of the CASSCF/MR-CCI calculations illustrated by the better agreement between calculated and experimental excitation energies at the CASPT2 level or solvent effects may explain the shift (3000 cm^{-1}) between the experimental and theoretical spectra. However, the main features of the experimental spectrum are reproduced by our model limited to a one-dimensional simulation.

IV. Conclusion

The relative position of the low-lying singlet MLCT ($3d_{Cr} \rightarrow \pi^*_{CO}$, $3d_{Cr} \rightarrow \pi^*_{bpy}$) and MC ($3d_{Cr} \rightarrow 3d_{Cr}$) excited states of $Cr(CO)_4$(bpy) as well as their oscillator strengths have been estimated through CASSCF calculations supplemented by MR-CCI and CASPT2 evaluation of the excitation energies for the $3d_{Cr} \rightarrow \pi^*_{bpy}$ MLCT and MC excited states.

Despite the high density of states which characterizes the absorption spectrum of this molecule, only a few states will play a key role at the early stage of the photodissociation dynamics. The main features of the experimental absorption spectrum, namely, an intense band in the visible around 20 000 cm^{-1} and a second band around 28 500 cm^{-1}, are reproduced with a blue shift of the theoretical spectrum of 3000 cm^{-1} with respect to the experimental one.

The photodissociation dynamics of the singlet MLCT ($3d_{Cr} \rightarrow \pi^*_{bpy}$) states belonging to the visible and near-UV energy domain have been investigated by wave packet propagation on one-dimensional potentials (q_a = $Cr-CO_{ax}$). The following mechanisms have been proposed:

After visible irradiation (500 nm: population of the b^1A_1 MLCT state), the molecule evolves along the b^1A_1 MLCT potential in an adiabatic process until complete dissociation of an axial carbonyl ligand with formation of the CO + $Cr(CO)_3$(bpy) primary products within 600 fs.

After UV irradiation (330 nm: population of the c^1A_1 and b^1B_1 states), 90% of the system gets trapped into the potential wells of the two MLCT states, whereas 10% dissociates in less than 500 fs in the b^1B_1 state. The dissociation probability reachs less than 15% in 1 ps.

The proposed mechanism accounts for the results of femtosecond spectroscopic measurements, namely, an ultrafast carbonyl departure in less than 600 fs. These results give an upper limit to the gas-phase rate of the photodissociation process but no account of the rate in solution. The femtosecond time-resolved spectroscopy points to a competitive trapping of the molecule in unreactive states. Moreover, the quantum yield dependence on the excitation wavelength and temperature in the visible energy domain indicates the presence of an energy barrier along the dissociative channel. This energy barrier appears to be high enough to trap a part of the system which can undergo very fast (<600 fs) nonradiative transitions to bound singlet or triplet states. The calculated potential corresponding to the b^1A_1 MLCT state presents a modest energy barrier, too small to prevent direct ultrafast dissociation. The present theoretical study restricted to a one-dimensional simulation (along the Cr−CO bond elongation) performed on non-coupled potentials can only give a qualitative picture of the photodissociation dynamics of $Cr(CO)_4$(bpy). Taking into account other degrees of freedom or solvent effects could modify significantly our conclusions regarding the branching ratio between reactive versus unreactive processes.

The observed photoreactivity, namely, a higher quantum yield of photosubstitution after UV irradiation, is not reproduced by the present simulation, which indicates probabilities of CO loss of 10% and 100% after absorption in the UV and visible, respectively. The quasibound character of the c^1A_1 and b^1B_1 MLCT states with respect to the $Cr-CO_{ax}$ bond elongation explains their low reactivity upon UV excitation.

The departure of an equatorial CO cannot be definitely ruled out. The experimentally determined structure of the solvated primary products CO + $Cr(CO)_3$(S)(bpy) seems to point to an axial carbonyl loss. However, the formation of the photosubstituted products is detected in the nanosecond time scale, which is beyond the ultrafast time scale of the carbonyl dissociation. A fac → mer rearrangement of the unsaturated fragment $Cr(CO)_3$(bpy) can, in principle, take place before or during the solvent coordination, although such a fast isomerization seems unlikely.

On the basis of these preliminary simulations, we have proposed a qualitative interpretation of the femtosecond time-resolved spectroscopy of $Cr(CO)_4$(bpy). The absorption spectrum has been assigned and the photoreactivity of the molecule upon visible irradiation has been attributed to the b^1A_1 MLCT ($3d_{xz} \rightarrow \pi^*_{bpy}$) state, directly accessible through visible irradiation, which acquires some MC character at dissociation. The time scale of the direct axial CO loss has been estimated to 600 fs, in agreement with the femtosecond experiments. Other reactive channels (equatorial CO loss), fac−mer rearrangement of the primary products, and influence of other degrees of freedom and environmental effects on the dynamics will be the subject of further investigations.

Acknowledgment. This work has been undertaken as part of the European collaborative COST project D4/0001/94. We thank the Département de Chimie of the CNRS for specific COST financial support. The calculations have been carried out either at the IDRIS (Orsay, France) through a grant of computer time from the Conseil Scientifique or at the LCQS (Strasbourg, France).

References and Notes

(1) (a) Van Dijk, H. K.; Servaas, P. C.; Stufkens, D. J.; Oskam, A. *Inorg. Chim. Acta* **1998**, *104*, 179. (b) Balk, R. W.; Snoeck, Th. L.; Stufkens, D. J.; Oskam, A. *Inorg. Chem.* **1980**, *19*, 3015. (c) Stufkens, D. J. *Coord. Chem. Rev.* **1990**, *104*, 39.

(2) Lindsay, E.; Vlček, A., Jr.; Langford, C. H. *Inorg. Chem*. **1993**, *32*, 2269.

(3) Stor, G. J.; Morrisson, S. L.; Stufkens, D. J.; Oskam, A. *Organometallics* **1994**, *13*, 2641.

(4) Rossenaar, B. D.; Lindsay, E.; Stufkens, D. J.; Vlček, A., Jr. *Inorg. Chim. Acta* **1996**, *250*, 5. Rossenaar, B. D.; Stufkens, D. J.; Oskam, A.; Fraanje, J.; Goubitz, K. *Inorg. Chim. Acta* **1996**, *247*, 215.

(5) Manuta, D. M.; Lees, A. J. *Inorg. Chem*. **1986**, *25*, 1354.

(6) Vichova, J.; Hartl, F.; Vlček, A. Jr. *J. Am. Chem. Soc.* **1992**, *114*, 10903.

(7) Vlček, A., Jr.; Vichova, J.; Hartl, F. *Coord. Chem. Rev.* **1994**, *132*, 167. Vlček, A., Jr. *Coord. Chem. Rev*. **1998**, *177*, 219. Farrell, I. R.; Vlček, A., Jr. *Chem. Rev*., in press.

(8) Vlček, A., Jr.; Grevels, F. W.; Snoeck, Th. L.; Stufkens, D. J. *Inorg. Chim. Acta* **1998**, *278*, 83.

(9) Virrels, I. C.; George, M. W.; Turner, J. J.; Peters, A.; Vlček, A., Jr. *Organometallics* **1996**, *15*, 4089.

(10) Fu, W.-F.; van Eldik, R. *Inorg. Chim. Acta* **1996**, *251*, 341; Wieland, S.; Reddy, K. B.; van Eldik, R. *Organometallics* **1990**, *9*, 1802. Fu, W.-F.; van Eldik, R. *Inorg. Chem*. **1998**, *37*, 1044.

(11) Guillaumont, D.; Daniel, C.; Vlček, A., Jr. *Inorg. Chem*. **1997**, *36*, 1684.

(12) Saito, H.; Fujita, J.; Saito, K. *Bull. Chem. Soc. Jpn*. **1968**, *41*, 359; 863.

(13) Farrell, I. R.; Matousek, P.; Vlček, A., Jr. *J. Am. Chem. Soc.* **1999**, *121*, 5296.
(14) Heitz, M. C.; Daniel, C. *J. Am. Chem. Soc*. **1997**, *119*, 8269.
(15) Heitz, M. C.; Finger, K.; Daniel, C. *Coord. Chem. Rev*. **1997**, *159*, 171. Guillaumont, D.; Daniel, C. *Coord. Chem. Rev.* **1998**, *181*, 177.
(16) Guillaumont, D.; Daniel, C. *J. Am. Chem. Soc.* **1999**, *121*, 11733.
(17) Rillence, D. P.; Jones, D. S.; Levy, H. A. *J. Chem. Soc., Chem. Commun.* **1979**, 849.
(18) Jost, A.; Rees, B.; Yelon, W. B. *Acta Crystallogr*. **1975**, *B31*, 2649.
(19) Kobayashi, H.; Kaizu, Y.; Kimura, H.; Matzuzawa, H.; Adachi, H. *Mol. Phys*. **1986**, *6*, 1009.
(20) Heitz, M. C.; Ribbing, C.; Daniel, C. *J. Chem. Phys*. **1997**, *106* (4), 1421.
(21) Pierloot, K.; Dumez, B.; Widmark, P.-O.; Roos, B. O. *Theor. Chim. Acta* **1995**, *90*, 87.
(22) Andersson, K.; Kello, V.; Lindh, R.; Malmqvist, P. -Å.; Noga, J.; Olsen, J.; Roos, B. O.; Sadlej, A. J.; Siegbahn, P. E. M.; Urban, M.; Widmark, P.-O. *Molcas 3.0*; University of Lund: Lund Sweden. The MR-CCI program is based on the original software developed by Siegbahn: Siegbahn, P. E. M. *Int. J. Quantum Chem*. **1983**, *23*, 1869.
(23) Marston, C. C.; Balint-Kurti, G. G. *J. Chem. Phys*. **1989**, *91*, 3571.
(24) Heller, E. J. *Acc. Chem. Res*. **1981**, *14*, 368. Heller, E. J. *J. Chem. Phys*. **1978**, *68*, 2066.
(25) Askar, A.; Cakmak, A. S. *J. Chem. Phys*. **1978**, *68*, 2794.
(26) Rosa, A.; Ricciardi, G.; Baerends, E. J.; Stufkens, D. J. *J. Phys. Chem*. **1996**, *100*, 15346.